

Implicit Integration for Articulated Bodies with Contact via the Nonconvex Maximal Dissipation Principle

Zherong Pan and Kris Hauser[†]

Abstract—We present non-convex maximal dissipation principle (NMDP), a time integration scheme for articulated bodies with simultaneous contacts. Our scheme resolves contact forces via the maximal dissipation principle (MDP). Prior MDP solvers compute contact forces via convex programming by assuming linearized dynamics integrated using the forward multistep scheme. Instead, we consider the coupled system of nonlinear Newton-Euler dynamics and MDP, which is time-integrated using the backward integration scheme. We show that the coupled system of equations can be solved efficiently using the projected gradient method with guaranteed convergence. We evaluate our method by predicting several locomotion trajectories for a quadruped robot. The results show that our NMDP scheme has several desirable properties including: (1) generalization to novel contact models; (2) superior stability under large timestep sizes; (3) consistent trajectory generation under varying timestep sizes.

I. INTRODUCTION

Articulated body simulation is an indispensable component of robot motion planning, optimal control, and reinforcement learning (RL). Their governing dynamic equations, i.e. the recursive Newton-Euler’s equation [9], and discretization schemes have been studied for decades. However, efficient and accurate contact handling is still a challenging problem studied extensively by recent works [28], [35]. To predict robot motions under simultaneous Coulomb frictional contacts, the two most widely-used formulations are the linear-complementary problem (LCP) [30] and the maximal dissipation principle (MDP) [7]. From a computational perspective, LCP incurs an NP-hard problem while MDP identifies contact forces with the solution of a cheap-to-compute convex program. As reported by [8], MDP-based contact handler achieves the best stability and computational efficiency. Moreover, MDP can encode novel contact models as arbitrary convex wrench spaces, which enables learning contact models from data [34], [35].

The stability region of MDP is shown to be up to ~ 10 ms according to [32]. Beyond the stability region, the predicted trajectory can either blow-up or drift significantly from the ground truth. Such small stability region not only increases computational cost but also induces problems of vanishing or exploding gradients [18]. In contact-implicit trajectory optimization [23], [29], for example, the problem sizes grow linearly with the number of timesteps and the cost of a Newton-type method grows superlinearly as a result.

We present a non-convex MDP (NMDP) integrator that: (1) is stable under large timestep sizes; (2) generates consistent contact forces under the MDP formulation; and (3)

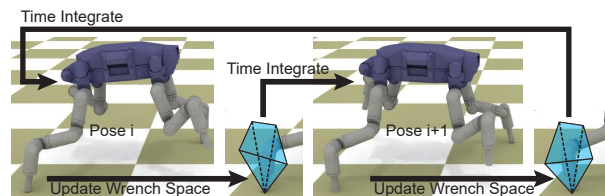


Fig. 1: We consider the three components (robot pose θ update, convex wrench space $v_x(\theta)$ update, and contact force w update) as a coupled system of nonlinear equations, which is solved using a novel projected gradient method with guaranteed convergence.

generalizes to position-dependent contact models. Prior MDP solvers rely on linearized dynamic systems, so that the kinetic energy becomes a quadratic function of the contact forces which can be solved as a convex QP. However, the truncation error of linearization can grow arbitrarily with larger timestep sizes. Our NMDP solver eliminates the truncation error by formulating the *nonlinear* recursive Newton-Euler’s equation and the wrench space as a function of the robot pose as a coupled system of nonlinear equations time-integrated using the backward-Euler scheme (Figure 1). The method can inherently account for novel contact models by using the convex shapes as feasible constraints in MDP, with nonlinear dependence on robot pose. To solve this coupled system we propose using the projected gradient method (PGM). We prove that PGM converges under sufficiently small timesteps and show that it empirically converges under large timesteps. An adaptive inner time-integration scheme guarantees that NMDP solves any (primary) timestep size in finite time.

We evaluate our method by predicting walking and jumping trajectories for the JPL Robosimian and Spider quadruped robot. The results show that NMDP has superior stability under larger timesteps as compared with conventional MDP solvers. In addition, the predicted walking speed and jumping height are more consistent under various timesteps.

II. RELATED WORK

We review related work on articulated body dynamics, contact handling, and generalized contact models.

Articulated Body Dynamics: Three classes of time discretization schemes have been independently developed for articulated bodies’ equation-of-motion. First, variational integrators (VI) [17], [20] discretize the Lagrangian function and then derive the discrete Euler-Lagrange equation. VI preserves momentum and energy symmetry under large timestep sizes. Second, linear multi-step integrators [6] discretize the equivalent Newton-Euler’s equation in the configuration space. These integrators are very efficient to evaluate using

[†] Zherong Pan and Kris Hauser are with the Department of Computer Science, University of Illinois at Urbana-Champaign. {zherong, kkhouser}@illinois.edu

the Articulated Body Algorithm (ABA) [9]. Third, high-order collocated, position-based integrators use an equivalent form of the Newton-Euler's equation known as position-based dynamics (PBD) [4], [26], where the main difference is that the discretization is performed in the Euclidean space. Position-based integrators are stable under large timestep sizes but they do not preserve symmetry.

Contact Handling: Sequential contact models [12], [22] have a significantly limited stability region due to the stiffness of contact forces. Models allowing simultaneous collisions and contacts have larger stability region, especially using implicit time stepper [1], [30]. LCP [2], [30] and MDP [7], [16] are the most popular implicit formulations for simultaneous frictional contacts. Solving complementary conditions due to LCP is NP-hard and can sometimes be infeasible [24]. The MDP relaxes the complementary constraints by allowing any contact forces in the frictional cone to be feasible. However, the stability region of time-stepper is still limited by the linearization of dynamic systems using either LCP or MDP. In [1], [26], dynamics with frictionless contacts are reformulated as an optimization and linearization can be avoided, but these results cannot be extended to frictional cases. In [25], the frictional force is modified and then reformulated as an optimization, but the modified variant cannot handle static-sliding frictional mode switches. In [5], a modified BDF2 scheme is proposed to achieve second-order accuracy in time-integration under frictional contacts, but linearization is still needed. Unlike these methods, we analyze the feasibility of contact handling without linearization for both normal and frictional forces.

Generalized Contact Models: Although the Coulomb frictional model is sufficient for most scenarios involving only rigid objects, other contact models are needed for several reasons. To model the unknown continuous force distribution between a planar object and a flat ground, a general convex wrench space is learned from real-world data in [34]. In other works [15], [19], [33], [35], articulated robots are walking on or swimming in deformable environments with granular or compliant materials. Hu [15] simulated both the granular material and the robot using fine-grained finite element method, which is more than 1000× slower than a standalone articulated body simulation. In [19], [33], the Coulomb frictional model is replaced with analytic and empirical force models. Although these models are cheap to compute, they cannot capture the static-sliding frictional mode switches. Zhu [35] used a similar approach as [34] and learned a robot-pose-dependent contact wrench space. Static-sliding frictional mode switches can thereby be modeled using MDP solver with the learned wrench space as constraints. By extending MDP, our NMDP solver can handle any generalized force models [34], [35] in the form of robot-pose-dependent contact wrench spaces.

III. ARTICULATED BODY DYNAMICS

In this section, we briefly review two prior formulations of articulated body dynamics and their corresponding discretization schemes: the recursive Newton-Euler's equation

and position-based dynamics. Both schemes can be extended to derive NMDP solvers.

A. Recursive Newton-Euler's Equation

The continuous Newton-Euler's equation under generalized coordinates takes the following form:

$$0 = H(\theta)\ddot{\theta} + C(\theta, \dot{\theta}) - \sum_{x \in \mathcal{C}} \nabla_{\theta} X(x, \theta)^T f_x - \tau. \quad (1)$$

Here H is the generalized mass matrix, θ is the robot's configuration vector, $C(\theta, \dot{\theta})$ is the Coriolis and Centrifugal force, $X(x, \theta)$ is the forward kinematic function bringing a point x from the robot's local coordinates to the global coordinates, \mathcal{C} is a set of points in contact with the environment, f_x is the external force on x in world coordinates, and finally τ is the joint torque.

Remark 1: We assume contacts are realized by external forces $f_x \in \mathbb{R}^3$. More general contact models such as [35] require external wrenches $f_x \in \mathbb{R}^6$. In this case, we can replace $\nabla_{\theta} X(x, \theta)$ with the Jacobian matrix in $\mathbb{R}^{6 \times |\theta|}$ and all the following analysis applies.

To discretize a dynamic system, the linear multistep method uses finite difference approximations for all variables. We illustrate this method with first-order finite difference schemes and higher-order schemes can be applied following a similar reasoning. We introduce two variables θ_- and θ_{--} . We assume that θ_- is the robot configuration at current time instance, θ_{--} is the robot configuration Δt seconds before (Δt is the timestep size), and θ is the to-be-predicted robot configuration after $\alpha \Delta t$ seconds. Here $\alpha \in (0, 1]$ is an additional parameter for timestep size control and we use subscripts to denote functions that are dependent on α . Since NMDP solver requires sufficiently small timestep sizes to converge, we use α to ensure this condition holds. Under these definitions, we can approximate:

$$\dot{\theta} \triangleq \frac{\theta - \theta_-}{\alpha \Delta t} \quad \dot{\theta}_- \triangleq \frac{\theta_- - \theta_{--}}{\Delta t} \quad \ddot{\theta} \triangleq \frac{\dot{\theta} - \dot{\theta}_-}{\Delta t}. \quad (2)$$

Plugging these approximations into the Newton-Euler's equation, the forward-Euler integrator takes the following form:

$$0 = H(\theta_-)\ddot{\theta} - C(\theta_-, \dot{\theta}_-) - \sum_{x \in \mathcal{C}} \nabla_{\theta} X(x, \theta_-)^T f_x - \tau, \quad (3)$$

which is a linearized dynamic system in θ, f_x, τ . Instead, the backward-Euler integrator evaluates H, C at time-level $\alpha \Delta t$ instead of current time instance, resulting in a nonlinear system of (1) and (2). This system is not guaranteed to have a solution, unless a small enough timestep size is used.

B. Position-Based Dynamics

PBD reformulates the governing equation-of-motion as:

$$0 = \nabla_{\theta} E_{\alpha}(\theta, f_x), \quad (4)$$

where we define:

$$E_{\alpha}(\theta, f) \triangleq I_{\alpha}(\theta) - \sum_{x \in \mathcal{C}} X(x, \theta)^T f_x - \theta^T \tau$$

$$I_{\alpha}(\theta) \triangleq \int_{x \in \mathcal{R}} \frac{\rho \|X(x, \theta) - (1 + \alpha)X(x, \theta_-) + \alpha X(x, \theta_{--})\|^2}{2\alpha \Delta t^2} dx,$$

and the integral in I_{α} is taken over the entire robot \mathcal{R} . If we assume that θ is a continuous trajectory $\theta(t)$ and $\theta =$

$\theta(t + \alpha\Delta t)$, $\theta_- = \theta(t)$, $\theta_{--} = \theta(t - \Delta t)$, it has been shown in [26] that (4) will converge to (1) as $\Delta t \rightarrow 0$. This integral can be evaluated analytically in a similar way as deriving the generalized mass matrix. By comparison with (1)+(2), (4) is always solvable under arbitrarily large timestep sizes because it is integrable. In other words, solving for θ is equivalent to the following optimization:

$$\underset{\theta}{\operatorname{argmin}} E_\alpha(\theta, f_x).$$

Note that we assume f_x is a constant in our derivation for the integrability of E_α (i.e. PBD dynamics can be written as $0 = \nabla_\theta E_\alpha(\theta, f_x)$ for some E_α). More generally, PBD can still take an integrable form when the external forces are conservative. In scenarios with dissipative force models such as Coulomb frictional forces, both integrability and PBD's feasibility guarantee are lost, just like Newton-Euler's equation. In this work, we propose an algorithm that solves the system of nonlinearity equations with dissipative force models with guaranteed solvability.

IV. NONCONVEX MDP

Our main idea is to combine backward time-integration and frictional contact force computation. In an MDP solver, the force at each contact point f_x belongs to a convex feasible space. We assume that the feasible space is a polytope with a set of vertices denoted as v_x^j with $j = 1, \dots, V_x$. Here V_x is the number of vertices used to model the polytope at contact point x . We assume that all the vertices v_x^j are assembled into a matrix $v_x = (v_x^1, \dots, v_x^{V_x})$ so feasible f_x is:

$$f_x \in \{v_x w_x \mid w_x \geq 0, \mathbf{1}^T w_x \leq 1\}, \quad (5)$$

where w_x is the weights of convex combination and $\mathbf{1}$ is an all-one vector.

Remark 2: The assumption of feasible contact force being a polytope is essential for our convergence proof. Under this assumption, we will extensively use the property that f_x has a bilinear form of $v_x w_x$, where w_x is bounded and v_x is sufficiently smooth.

A. NMDP Formulation

When modeling an inelastic rigid contact, v_x is set to the vertices of the linearized frictional cone if $X(x, \theta)$ is in contact or penetrating the environment, and v_x is set to zero otherwise. However, the switch between the in-contact and off-contact state is non-differentiable which is undesirable in applications such as differential dynamic programming [32] and trajectory optimization [23]. Therefore, we assume that v_x is a robot-pose-dependent, differentiable function $v_x(\theta)$. This formulation is compatible with the recently proposed learning-based granular wrench space model [35] and can potentially generalize to other contact models. To determine the weights w_x , MDP solves an optimization that minimizes the kinetic energy at time instance $\alpha\Delta t$. Conventional MDP solver uses the linearized dynamic system Equation 3 and discretizes v_x at θ_- , resulting in a QP problem. Instead, our NMDP scheme uses the backward-Euler integrator Equation 1 and discretizes v_x at θ . As a result, we need to solve

the following nonlinear constrained optimization:

$$\begin{aligned} \underset{\theta, w}{\operatorname{argmin}} K(\theta) \quad \text{s.t. } 0 &= G_\alpha(\theta, w) \\ K(\theta) &\triangleq \frac{1}{2} \dot{\theta}^T H(\theta) \dot{\theta} \\ G_\alpha(\theta, w) &\triangleq H(\theta) \ddot{\theta} + C(\theta, \dot{\theta}) - \\ &\sum_{x \in \mathcal{C}} \nabla_\theta X(x, \theta)^T v_x(\theta) w_x - \tau, \end{aligned} \quad (6)$$

where we assume the use of recursive Newton-Euler's equation and w is a concatenation of all w_x . In the rest of the paper, we propose two algorithms to solve (6) and analyze their convergence.

B. NMDP Solver

Since (6) is a general nonlinear constrained optimization, it can be solved using general-purpose optimizers such as the interior point method [21]. However, these methods are not guaranteed to converge to a first-order stationary point due to infeasibility. Instead, we consider two variants of the projected gradient method (PGM), which we prove to converge to a first order stationary point. PGM starts from a feasible initial guess and updates a search direction of w by solving:

$$\underset{\Delta\theta, \Delta w}{\operatorname{argmin}} K(\theta + \Delta\theta) \quad \text{s.t. } G_\alpha(\theta + \Delta\theta, w + \Delta w) = 0 \quad (7)$$

$$K(\theta + \Delta\theta) \triangleq K(\theta) + \nabla_\theta K^T \Delta\theta + \frac{1}{2} \Delta\theta \nabla_\theta^2 K \Delta\theta$$

$$G_\alpha(\theta + \Delta\theta, w + \Delta w) \triangleq \nabla_\theta G_\alpha \Delta\theta + \nabla_w G \Delta w.$$

If $\nabla_\theta G_\alpha$ is non-singular, then (7) is equivalent to the following QP:

$$\underset{\Delta w}{\operatorname{argmin}} -\nabla_\theta K^T \nabla_\theta G_\alpha^{-1} \nabla_w G \Delta w + \|w\|^2 / \gamma \quad (8)$$

$$\frac{1}{2} \Delta w^T \nabla_w G^T \nabla_\theta G_\alpha^{-T} \nabla_\theta^2 K \nabla_\theta G_\alpha^{-1} \nabla_w G \Delta w$$

$$\text{s.t. } (w + \Delta w) \geq 0, \mathbb{1}^T (w + \Delta w) \leq 1,$$

where we use γ to facilitate line search. The matrix $\mathbb{1}$ is a concatenation of constraints that w_x sums to less than one on each contact point x . After solving for a new $w \leftarrow w + \Delta w$, we update θ by projecting it to the $G_\alpha(\theta, w) = 0$ manifold using the following recursion:

$$\theta \leftarrow \theta - \nabla_\theta G_\alpha^{-1} G_\alpha(\theta, w). \quad (9)$$

Note that we have only used the first-order derivatives of G_α in (8) so the PGM has linear convergence speed at best. Our second version of PGM differs in that we ignore all gradients of the function v_x , i.e. zeroth-order update for v_x . This requirement is inspired by the recent work [35] where the contact wrench space is learned from real-world data. In this case, computing derivatives of v_x involves costly back-propagation through a learning model, e.g. neural networks, sublevel sets of high-order polynomials [34], or radial basis functions [35]. Mathematically, the derivatives of v_x only occurs in $\nabla_\theta G_\alpha$ and we denote its zeroth-order, inexact variant as:

$$\nabla_\theta \bar{G}_\alpha(\theta, w) \triangleq \nabla_\theta G_\alpha(\theta, w) + \sum_{x \in \mathcal{C}} \nabla_\theta X(x, \theta)^T \nabla_\theta v_x(\theta) w_x.$$

Using $\nabla_{\theta}\bar{G}_{\alpha}$, we derive the following, inexact counterpart of QP (Equation 8):

$$\begin{aligned} \underset{\Delta w}{\operatorname{argmin}} \quad & -\nabla_{\theta}K^T\nabla_{\theta}\bar{G}_{\alpha}^{-1}\nabla_wG\Delta w + \|w\|^2/\gamma \quad (10) \\ & \frac{1}{2}\Delta w^T\nabla_wG^T\nabla_{\theta}\bar{G}_{\alpha}^{-T}\nabla_{\theta}^2K\nabla_{\theta}\bar{G}_{\alpha}^{-1}\nabla_w\bar{G}_{\alpha}\Delta w \\ \text{s.t.} \quad & (w + \Delta w) \geq 0, \mathbb{1}^T(w + \Delta w) \leq 1, \end{aligned}$$

and the following, inexact counterpart of manifold projection (Equation 9):

$$\theta \leftarrow \theta - \nabla_{\theta}\bar{G}_{\alpha}^{-1}G_{\alpha}(\theta, w). \quad (11)$$

The pipeline of both first- and zeroth-order PGM is outlined in Algorithm 1.

Algorithm 1: (First- / Zeroth-) Order PGM($\alpha, \Delta t, \theta_-, \theta_-$)

```

1:  $w^0 \leftarrow 0, \theta^0 \leftarrow \theta_-, \gamma^0 \leftarrow 1, \eta > 1$ 
2: while  $\|G_{\alpha}(\theta^0, w^0)\| \neq 0$  do
3:   Compute (9) or (11) ( $\theta = \theta^0, w = w^0$ )
4: for  $k = 1, \dots$  do
5:   Solve (8) or (10) ( $\theta = \theta^{k-1}, w = w^{k-1}$ ) for  $w^k$ 
6:    $\theta^k \leftarrow \theta^{k-1}$ 
7:   while  $\|G_{\alpha}(\theta^k, w^k)\| \neq 0$  do
8:     Compute (9) or (11) ( $\theta = \theta^k, w = w^k$ )
9:     if  $K(\theta^k) > K(\theta^{k-1})$  then
10:       $\gamma \leftarrow \eta\gamma, \theta^k \leftarrow \theta^{k-1}, w^k \leftarrow w^{k-1}$ 
11:     else
12:        $\gamma \leftarrow \gamma/\eta$ 
13:       if  $\|\theta^k - \theta^{k-1}\|_{\infty} < \epsilon$  then
14:         Return  $\theta^k, w^k$ 

```

V. CONVERGENCE ANALYSIS

We analyze the convergence of Algorithm 1 in both first- and zeroth-order cases. PGM cannot proceed if $\nabla_{\theta}G_{\alpha}$ is rank-deficient and does not have an inverse. In addition, the manifold projection substeps in PGM can diverge without using line-search strategies. Finally, the outer-loop of the zeroth-order PGM can fail to converge by using an inexact gradient. We take the following three assumptions to show that first-order PGM and zeroth-order manifold projection are well-defined and convergent:

A 5.1: $X \in \mathcal{C}^{\infty}$.

A 5.2: $\sigma_{\min} \left[\int_{x \in \mathcal{R}} \frac{\rho}{\Delta t^2} \nabla_{\theta}X^T \nabla_{\theta}X dx \right] (\theta_-) \geq \sigma_X > 0$.

A 5.3: $\frac{\partial^3 v_x}{\partial \theta^3} \in \mathcal{C}^0$.

To show that zeroth-order PGM is also convergent, we need an additional assumption:

A 5.4: $\nabla_w G$ has full row rank.

Remark 3: A 5.1 and A 5.2 can be satisfied by choosing appropriate parameterizations of robot joints. When all the hinge joints are parameterized using Euler angles, then A 5.1 is satisfied. A 5.2 requires that the kinetic energy $K(\theta)$ is strictly convex at θ_- . In other words, for any infinitesimal perturbation $\delta\theta$, there must be some points $x \in \mathcal{R}$ undergoing infinitesimal movements δx with non-vanishing $\lim_{\delta\theta \rightarrow 0} \delta x / \delta\theta$. This assumption can only be violated when the robot is suffering from Gimbal lock of Euler angles, which can be easily resolved by moving the singular point away from the current configuration.

Remark 4: A 5.3 indicates that NMDP can only handle smooth contact force models. Stiff and penetration-free

contacts between two rigid objects cannot be handled by our method. However, smooth force models are essential for gradient-based motion planning and control [23], [27], [32]. In addition, stiff contacts can be approximated by smooth contacts. For example, a linearized frictional cone is a polytope with vertices being $v_x^i = n + t^i \mu$, where n is the contact normal and t^i is a direction on the tangential plane. We modify this definition to satisfy A 5.3 by setting $v_x^i = d(X(x, \theta))^3 (n + t^i \mu)$, where $d(X(x, \theta))$ is the penetration depth of the contact point x . This force model can be made arbitrarily stiff by scaling v_x^i with a big constant.

Remark 5: A 5.4 is a major limitation of the zeroth-order PGM. Note that $v_x = 0$ and thus $\nabla_w G$ has a zero rank when a contact point x does not penetrate the environment. However, once the penetration depth becomes non-zero, then $v_x \neq 0$ and $\nabla_w G$ can have a full row rank. A 5.4 disallows such jumps in the rank of $\nabla_w G$. A simple workaround is to slightly modify the contact model by allowing small, non-zero contact forces even when robot is not in contact with the environment. One method to satisfy A 5.4 is to set $v_x^i = (d(X(x, \theta))^3 + \zeta)(n + t^i \mu)$, where ζ is a small positive constant. In our implementation, we ignore A 5.4 and have never observed divergence behavior due to the violation of this assumption.

Under the above assumptions, our main results are:

Theorem 5.5 (First-Order PGM Convergence):

Assuming A 5.1, A 5.2, A 5.3, there exists $\alpha_4 > 0$, such that for all $\alpha \leq \alpha_4$, the first order Algorithm 1 will generate a monotonically decreasing sequence of $\{K(\theta^k)\}$ where each θ^k satisfies $G(\theta^k, w^k) = 0$.

Theorem 5.6 (Zeroth-Order PGM Convergence):

Assuming A 5.1, A 5.2, A 5.3, A 5.4, there exists $\alpha_5 > 0$, such that for all $\alpha \leq \alpha_5$, the zeroth-order Algorithm 1 will generate a monotonically decreasing sequence of $\{K(\theta^k)\}$ where each θ^k satisfies $G(\theta^k, w^k) = 0$.

The proofs of these results are deferred to Section IX. Both results imply that timestep sizes cannot be arbitrarily large, otherwise PGM can fail to converge. In addition, the divergence behavior of PGM can only happen in the manifold projection substep when the norm $\|G_{\alpha}\|, \|\bar{G}_{\alpha}\|$ does not decrease after apply Equation 9 or Equation 11, which is an indicator of the use of smaller timestep sizes. As a result, we can design a robust articulated body simulator using adaptive timestep control as illustrated in Algorithm 2.

Algorithm 2 starts by time-integrating using $\alpha = 1$. If PGM diverges, we cut the timestep size by half, i.e. setting $\alpha = 0.5$ and recurse. Note that $\text{simulate}(\alpha, \Delta t, \theta_-, \theta_-)$ implies 1) the last timestep size is Δt and 2) the desired next time instance is $\alpha\Delta t$ ahead. If PGM diverges, we slice timestep size by half and call $\text{simulate}(\alpha/2, \Delta t/2, \theta_-, \theta_-)$ for the first half. However, further subdivision might happen for the first half due to recursion, so we return the last timestep size, say Δt^* . Next, we time integrate the second half. Given that last timestep size is Δt^* and our desired $\alpha^* \Delta t^* = \alpha\Delta t/2$, we must have $\alpha^* = (\alpha\Delta t)/(2\Delta t^*)$.

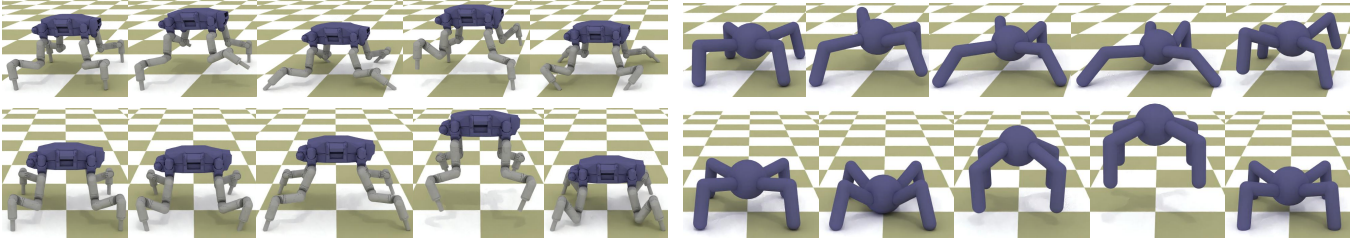


Fig. 2: The robots’ walking (top) and jumping (bottom) trajectories tracked using the stable PD controller and simulated using our NMDP solver, where we use $\Delta t = 0.05s$.

Algorithm 2: $\text{simulate}(\alpha, \Delta t, \theta_-, \theta_{--})$

```

1:  $\theta, w \leftarrow \text{PGM}(\alpha, \Delta t, \theta_-, \theta_{--})$ 
2: if Converged then
3:   Return  $\alpha \Delta t, \theta, \theta_-$ 
4: else
5:    $\Delta t^*, \theta^*, \theta_-^* \leftarrow \text{simulate}(\alpha/2, \Delta t, \theta_-, \theta_{--})$ 
6:    $\alpha^* \leftarrow (\alpha \Delta t) / (2 \Delta t^*)$ 
7:    $\Delta t^{**}, \theta^{**}, \theta_-^{**} \leftarrow \text{simulate}(\alpha^*, \Delta t^*, \theta^*, \theta_-^*)$ 
8:   Return  $\Delta t^{**}, \theta^{**}, \theta_-^{**}$ 

```

A. NMDP Working with PBD

Our analysis and formulation assumes the use of Newton-Euler’s equation. An equivalent form of NMDP can be formulated for the position-based dynamics via a new definition of $K(\theta)$ and G_α as follows:

$$\begin{aligned} & \underset{\theta, w}{\text{argmin}} K(\theta) \quad \text{s.t. } 0 = G_\alpha(\theta, w) \\ K(\theta) & \triangleq \int_{x \in \mathcal{R}} \frac{\rho \|X(x, \theta) - X(x, \theta_-)\|^2}{2\Delta t^2} dx \\ G_\alpha & \triangleq \nabla_\theta I_\alpha(\theta) - \sum_{x \in \mathcal{C}} \nabla_\theta X(x, \theta)^T v_x(\theta) w_x - \tau, \end{aligned} \quad (12)$$

and all the convergence analysis applies to Equation 6 and Equation 12 alike. We refer readers to Section IX for all the proof.

VI. EVALUATIONS

We evaluate the performance of NMDP in various scenarios. We implement both versions of NMDP (Equation 6 and Equation 12) using C++ and Eigen [13], where the optimizations can be solved using both first- and zeroth-order PGM. All the matrix inversions in manifold projection are solved by a rank-revealing LU factorization. As long as the factorization detects that the matrix is near singular (i.e. A 5.2 is violated) or the norm $\|G_\alpha\|, \|\bar{G}_\alpha\|$ does not decrease, we restart PGM with smaller timestep sizes. In each outer loop of PGM, a QP is solved and the problem data of these QP are quite similar. We use the parametric QP solver [10] that can make use of these similarities to accelerate computation. Finally, we set $\epsilon = 10^{-6}, \eta = 1.5, \zeta = 10^{-3}$.

As illustrated in Figure 2, we conduct experiments on the Robosimian by having different simulators to track a prescribed robot walking or jumping trajectory using the stable PD controller [31]. The stable PD controller is consistent with the backward-Euler integrator, which uses $\theta, \dot{\theta}$ instead of $\theta_-, \dot{\theta}_-$ as the target state to be tracked. We compare the performance of the following simulators:

- NE-NMDP-PGM/NE-NMDP-ZOPGM: Equation 6 solved using first-/zeroth-order PGM.
- PBD-NMDP-PGM/PBD-NMDP-ZOPGM: Equation 12 solved using first-/zeroth-order PGM.
- NE-MDP: linearized Newton-Euler’s equation with contact forces solved using MDP.

Stability Under Large Timestep Sizes: We track a robot jumping trajectory that uses symmetric poses. Since the Robosimian’s body shape is also symmetric, the torso in the tracked trajectory should have zero tilt angles from the vertical axis, which is our groundtruth. In Figure 3 (ab), we plot the torso’s tile angle predicted by NE-MDP and NE-NMDP-PGM under different timestep sizes. NE-MDP is only stable when $\Delta t \leq 7ms$ and the simulator explodes under larger Δt . Even when $\Delta t \leq 7ms$, the tile angle suffers from severe oscillation. In comparison, NE-NMDP-PGM is stable when Δt increases from 5ms to 50ms and the predicted tile angle oscillation is relatively small. We further plot the tile angle sequence predicted by the other three variants of PGM in Figure 3 (cde), the oscillations are consistently small. When using PGM with $\Delta t \leq 50ms$, we have never experienced any divergence behaviors so Algorithm 2 is never needed. But divergence happens in ZOPGM and we observe larger tile angle oscillation in Figure 3 (ce).

Consistent Prediction: The tracked robot jumping trajectory lasts for 10 seconds with 5 repeated jumping behaviors. As a result, the expected torso height should be a periodic function. In Figure 4, we plot the torso height trajectory predicted using the five methods. With $\Delta t \leq 7ms$, the trajectories generated by NE-MDP are suffering from relatively large variations. While all four PGM variants can consistently predict a periodic function when Δt increases from 5ms to 50ms. A similar result is observed in the walking trajectory. As shown in Figure 5, the groundtruth walking distance is a linear function of time. The trajectories predicted using NE-MDP exhibit a large variations with different timestep sizes. The consistency of NE-NMDP-(ZO)PGM are much better and that of PBD-NMDP-(ZO)PGM are the best. Compared with NE-NMDP-(ZO)PGM, the additional stability and consistency of PBD-NMDP-(ZO)PGM are presumably due to the fact that Euclidean space discretization is more accurate than that in the configuration space [26].

Computational Cost: We summarize the computational performance by collecting and analyzing all the timesteps in the four trajectories of Figure 2 simulated at $\Delta t = 50ms$. Figure 6 (a) profiles the instantaneous framerate, of which MDP is the most efficient involving a single QP solve.

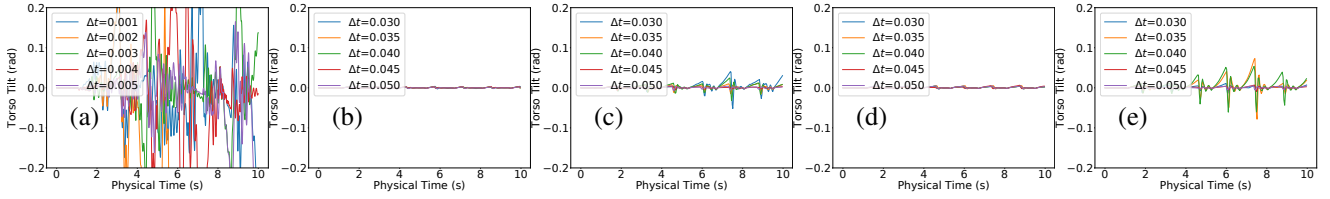


Fig. 3: The torso tilt of the tracked jumping trajectory. (a): NE-MDP (b): NE-NMDP-PGM (c): NE-NMDP-ZOPGM (d): PBD-NMDP-PGM (e): PBD-NMDP-ZOPGM

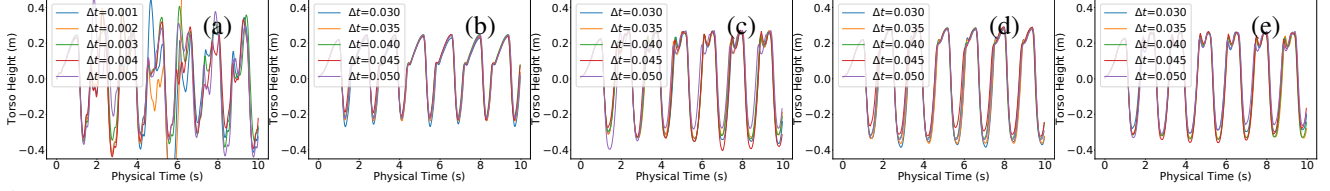


Fig. 4: The torso height of the tracked jumping trajectory. (a): NE-MDP (b): NE-NMDP-PGM (c): NE-NMDP-ZOPGM (d): PBD-NMDP-PGM (e): PBD-NMDP-ZOPGM

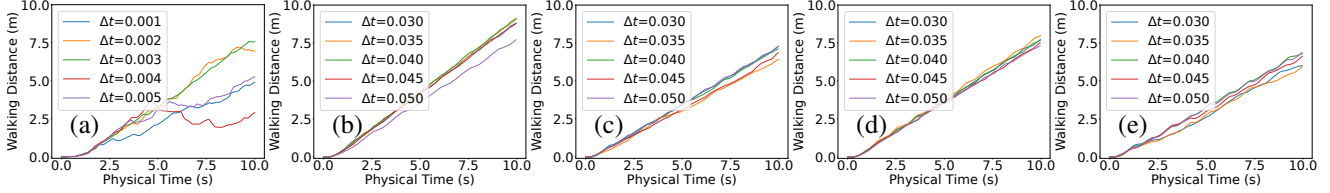


Fig. 5: The distance of the tracked walking trajectory. (a): NE-MDP (b): NE-NMDP-PGM (c): NE-NMDP-ZOPGM (d): PBD-NMDP-PGM (e): PBD-NMDP-ZOPGM

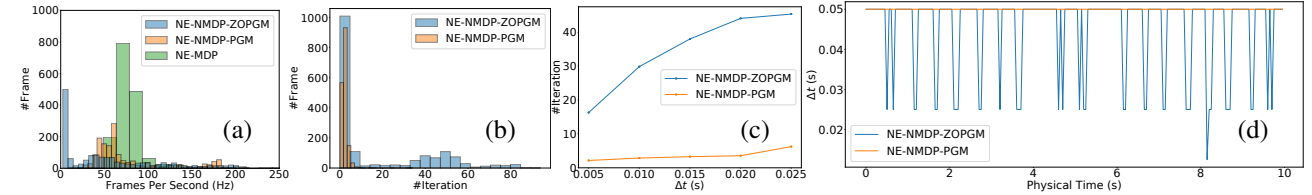


Fig. 6: A performance comparison of different methods. (a): Histogram of framerates (b): Histogram of number of outer iterations per frame (c): Number of outer iterations against Δt (d): Adaptive timestep size

PGM does not incur a significant sacrifice in framerate while ZOPGM is significantly slower. Figure 6 (b) profiles the number of outer iterations of Algorithm 1 until convergence and Figure 6 (c) plots the average number of outer iterations against Δt . These figures show that ZOPGM is an approximately one order of magnitude slower than PGM, but ZOPGM provides the extra convenience that analytic derivatives of $v_x(\theta)$ is not needed. Finally, Figure 6 (d) shows the smallest timestep size chosen by Algorithm 2 for PGM and ZOPGM. At $\Delta t = 50\text{ms}$, PGM is always convergent. ZOPGM is convergent for most timesteps, but Δt needs to get down to 25ms during some critical time instances (e.g. when robot changes contact state).

VII. CONCLUSION & DISCUSSION

We present NMDP, a backward-Euler time integration scheme for articulated bodies under generalized contact models. The key to our formulation is the representation of contact forces as a convex combination of vertices of the feasible contact wrench space. To model generalized contact models, we assume that these vertices are dependent on the robot pose. Following the idea of backward-Euler time integrator, we discretize both the articulated body dynamics and the vertices of contact wrench spaces at the next time

instance instead of the current one. We solve the constrained optimization using a projected gradient method. Our analysis proves that NMDP has guaranteed convergence under small timestep sizes and a robust simulator can be built using an adaptive timestep size control algorithm. Empirically, we show that this scheme has better stability under large timestep sizes and consistency over varying timestep sizes.

We plan to address several limitations in our future work. First, the main idea of NMDP is not limited to articulated bodies and can be extended to high-dimensional dynamic systems such as deformable objects. However, it requires exact inversion of the constraint Jacobian, which is impractical in high-dimensional scenarios. Second, we assume a small set of known contact points. When new contacts are detected, we do not handle them in our implementation. Third, the generalized contact model needs to be smooth and cannot provide collision-free guarantees. Finally, we plan to evaluate the performance of optimization-based motion planners and controllers using NMDP as the underlying integration model.

VIII. ACKNOWLEDGEMENT

This work is partially funded by NSF Grant #1911087 and authors thank Mengchao Zhang for proofreading the paper.

REFERENCES

- [1] M. Anitescu, "A fixed time-step approach for multibody dynamics with contact and friction," in *Proceedings 2003 IEEE/RSJ International Conference on Intelligent Robots and Systems (IROS 2003)* (Cat. No.03CH37453), vol. 4, 2003, pp. 3725–3731 vol.3.
- [2] M. Anitescu, "Optimization-based simulation of nonsmooth rigid multibody dynamics," *Mathematical Programming*, vol. 105, no. 1, pp. 113–143, 2006.
- [3] J.-P. Aubin, *Viability Theorems for Ordinary and Stochastic Differential Equations*. Boston, MA: Birkhäuser Boston, 2009, pp. 19–52.
- [4] J. Bender, M. Müller, and M. Macklin, "A Survey on Position Based Dynamics," in *EG 2017 - Tutorials*, A. Bousseau and D. Gutierrez, Eds. The Eurographics Association, 2017.
- [5] G. E. Brown, M. Overby, Z. Foroootaninia, and R. Narain, "Accurate dissipative forces in optimization integrators," *ACM Trans. Graph.*, vol. 37, no. 6, Dec. 2018. [Online]. Available: <https://doi.org/10.1145/3272127.3275011>
- [6] J. C. Butcher and N. Goodwin, *Numerical methods for ordinary differential equations*. Wiley Online Library, 2008, vol. 2.
- [7] E. Drumwright and D. A. Shell, "Modeling contact friction and joint friction in dynamic robotic simulation using the principle of maximum dissipation," in *Algorithmic foundations of robotics IX*. Springer, 2010, pp. 249–266.
- [8] T. Erez, Y. Tassa, and E. Todorov, "Simulation tools for model-based robotics: Comparison of bullet, havok, mujoco, ode and physx," in *2015 IEEE international conference on robotics and automation (ICRA)*. IEEE, 2015, pp. 4397–4404.
- [9] R. Featherstone, *Rigid body dynamics algorithms*. Springer, 2014.
- [10] H. J. Ferreau, C. Kirches, A. Potschka, H. G. Bock, and M. Diehl, "qpooases: A parametric active-set algorithm for quadratic programming," *Mathematical Programming Computation*, vol. 6, no. 4, pp. 327–363, 2014.
- [11] G. H. Golub and C. F. Van Loan, *Matrix Computations*, 3rd ed. The Johns Hopkins University Press, 1996.
- [12] E. Guendelman, R. Bridson, and R. Fedkiw, "Nonconvex rigid bodies with stacking," *ACM transactions on graphics (TOG)*, vol. 22, no. 3, pp. 871–878, 2003.
- [13] G. Guennebaud, B. Jacob, et al., "Eigen v3," <http://eigen.tuxfamily.org>, 2010.
- [14] R. A. Horn, R. A. Horn, and C. R. Johnson, *Topics in matrix analysis*. Cambridge university press, 1994.
- [15] Y. Hu, Y. Fang, Z. Ge, Z. Qu, Y. Zhu, A. Pradhana, and C. Jiang, "A moving least squares material point method with displacement discontinuity and two-way rigid body coupling," *ACM Transactions on Graphics (TOG)*, vol. 37, no. 4, pp. 1–14, 2018.
- [16] D. M. Kaufman, S. Sueda, D. L. James, and D. K. Pai, "Staggered projections for frictional contact in multibody systems," in *ACM SIGGRAPH Asia 2008 papers*, 2008, pp. 1–11.
- [17] J. Lee, C. K. Liu, F. C. Park, and S. S. Srinivasa, "A linear-time variational integrator for multibody systems," in *Algorithmic Foundations of Robotics XII*. Springer, 2020, pp. 352–367.
- [18] G.-H. Liu, T. Chen, and E. A. Theodorou, "Differential dynamic programming neural optimizer," *arXiv preprint arXiv:2002.08809*, 2020.
- [19] R. D. Maladen, Y. Ding, P. B. Umbanhowar, A. Kamor, and D. I. Goldman, "Biophysically inspired development of a sand-swimming robot," in *Robotics: Science and Systems*. Georgia Institute of Technology, 2011.
- [20] J. Marsden and M. West, "Discrete mechanics and variational integrators," *Acta Numerica*, vol. 10, no. 5, pp. 357–514, 2001.
- [21] S. Mehrotra, "On the implementation of a primal-dual interior point method," *SIAM Journal on optimization*, vol. 2, no. 4, pp. 575–601, 1992.
- [22] B. V. Mirtich, *Impulse-based dynamic simulation of rigid body systems*. University of California, Berkeley, 1996.
- [23] I. Mordatch, E. Todorov, and Z. Popović, "Discovery of complex behaviors through contact-invariant optimization," *ACM Transactions on Graphics (TOG)*, vol. 31, no. 4, pp. 1–8, 2012.
- [24] P. Painlevé, "Sur les lois du frottement de glissement," *Nonlinear Dynamics*, vol. 8, no. 5, pp. 977–979, 2012.
- [25] Z. Pan and D. Manocha, "Position-based time-integrator for frictional articulated body dynamics," in *2018 IEEE/RSJ International Conference on Intelligent Robots and Systems (IROS)*, 2018, pp. 1–8.
- [26] Z. Pan and D. Manocha, "Time Integrating Articulated Body Dynamics Using Position-Based Collocation Methods," in *Algorithmic Foundations of Robotics XIII*, M. Morales, L. Tapia, G. Sánchez-Ante, and S. Hutchinson, Eds. Cham: Springer International Publishing, 2020, pp. 673–688.
- [27] Z. Pan, B. Ren, and D. Manocha, "Gpu-based contact-aware trajectory optimization using a smooth force model," in *Proceedings of the 18th Annual ACM SIGGRAPH/Eurographics Symposium on Computer Animation*, ser. SCA '19. New York, NY, USA: Association for Computing Machinery, 2019. [Online]. Available: <https://doi.org/10.1145/3309486.3340246>
- [28] T. Preclik, S. Eibl, and U. Rude, "The maximum dissipation principle in rigid-body dynamics with inelastic impacts," *Computational Mechanics*, vol. 62, no. 1, pp. 81–96, 2018.
- [29] J. Sleiman, J. Carius, R. Grandia, M. Wermelinger, and M. Hutter, "Contact-implicit trajectory optimization for dynamic object manipulation," in *2019 IEEE/RSJ International Conference on Intelligent Robots and Systems (IROS)*, 2019, pp. 6814–6821.
- [30] D. E. Stewart, "Rigid-body dynamics with friction and impact," *SIAM review*, vol. 42, no. 1, pp. 3–39, 2000.
- [31] J. Tan, K. Liu, and G. Turk, "Stable proportional-derivative controllers," *IEEE Computer Graphics and Applications*, vol. 31, no. 4, pp. 34–44, 2011.
- [32] Y. Tassa, T. Erez, and E. Todorov, "Synthesis and stabilization of complex behaviors through online trajectory optimization," in *2012 IEEE/RSJ International Conference on Intelligent Robots and Systems*. IEEE, 2012, pp. 4906–4913.
- [33] V. Vasilopoulos, I. S. Paraskevas, and E. G. Papadopoulos, "Compliant terrain legged locomotion using a viscoplastic approach," in *2014 IEEE/RSJ International Conference on Intelligent Robots and Systems*, 2014, pp. 4849–4854.

- [34] J. Zhou, M. T. Mason, R. Paolini, and D. Bagnell, "A convex polynomial model for planar sliding mechanics: theory, application, and experimental validation," *International Journal of Robotics Research*, 2018.
- [35] Y. Zhu, L. Abdulmajeid, and K. Hauser, "A data-driven approach for fast simulation of robot locomotion on granular media," in *2019 International Conference on Robotics and Automation (ICRA)*, 2019, pp. 7653–7659.

IX. APPENDIX: PROOF

We define some convenient shorthand notations.

$$G_\alpha(\theta, w) = \frac{1}{\alpha} A(\theta) + B(\theta, w)$$

$$A(\theta) = \int_{x \in \mathcal{R}} \frac{\rho}{\Delta t^2} \nabla_\theta X^T (X(x, \theta) - X(x, \theta_-)) dx$$

$$B(\theta, w) = \int_{x \in \mathcal{R}} \frac{\rho}{\Delta t^2} \nabla_\theta X^T (X(x, \theta_-) - X(x, \theta_-)) dx - \sum_{x \in \mathcal{C}} \nabla_\theta X(x, \theta)^T v_x(\theta) w_x - \tau.$$

Note that all variables or functions that depend on α will be labeled using a subscript, and vice versa.

A. Continuous Manifold Projection

We begin our analysis by showing that θ satisfying $G_\alpha(\theta, w) = 0$ can be arbitrarily close to θ_- by using sufficiently small α . This can be proved by analyzing the following Lyapunov candidate:

$$V_\alpha(\theta, w) = \|G_\alpha(\theta, w)\|^2 = \frac{1}{\alpha^2} A^T A + \frac{2}{\alpha} A^T B + B^T B.$$

We prove basic properties of boundedness and convexity:

Lemma 9.1: Assuming A 5.1, A 5.2, A 5.3, there exists an $r > 0$, such that for all feasible w , the following properties hold within $\mathcal{B}(\theta_-, r)$:

- 1) $\sigma_{\min}(\nabla_\theta G_\alpha) \geq \frac{\sigma_X}{2\alpha} - \sigma_B.$
- 2) $\sigma_{\min}(\nabla_\theta^2 V_\alpha) \geq \frac{\sigma_X}{2\alpha^2} - \frac{2}{\alpha} \sigma_{AB} - \sigma_{BB}.$
- 3) $\|\nabla_\theta G_\alpha\| \leq \frac{1}{\alpha} M_A^1 + M_B^1.$
- 4) $\|\nabla_\theta^2 G_\alpha\| \leq \frac{1}{\alpha} M_A^2 + M_B^2.$
- 5) $\|\nabla_\theta V_\alpha\| \leq \frac{1}{\alpha^2} M_{AA}^1 + \frac{1}{\alpha} M_{AB}^1 + M_{BB}^1.$
- 6) $\|\nabla_\theta^2 V_\alpha\| \leq \frac{1}{\alpha^2} M_{AA}^2 + \frac{1}{\alpha} M_{AB}^2 + M_{BB}^2.$
- 7) $\|\nabla_\theta^3 V_\alpha\| \leq \frac{1}{\alpha^2} M_{AA}^3 + \frac{1}{\alpha} M_{AB}^3 + M_{BB}^3.$
- 8) $\|\nabla_\theta V_\alpha(\theta_-, w)\| \leq \frac{1}{\alpha} M_{AG} + M_{BG}.$
- 9) $\|G_\alpha(\theta_-, w)\| \leq M_G.$
- 10) $\|B(\theta, w) - B(\theta', w')\| \leq M_{\Delta B}.$

Proof: These are immediate results of continuity of functions and singular values of matrices. **1):**

$$\begin{aligned} & \sigma_{\min}(\nabla_\theta G_\alpha) \\ &= \sigma_{\min}\left(\frac{1}{\alpha} \nabla_\theta A + \nabla_\theta B\right) \\ &\geq \sigma_{\min}\left(\frac{1}{\alpha} \nabla_\theta A\right) - \sigma_{\max}(\nabla_\theta B) \quad ([14, \text{Equation 3.3.17}]) \\ &\geq \sigma_{\min}\left(\frac{1}{2\alpha} \nabla_\theta A(\theta_-)\right) - \sigma_{\max}(\nabla_\theta B) \quad ([11, \text{Corollary 8.6.2}], A 5.1) \\ &\geq \frac{\sigma_X}{2\alpha} - \sigma_{\max}(\nabla_\theta B) \quad (A 5.2) \\ &\geq \frac{\sigma_X}{2\alpha} - \sigma_B. \quad ([11, \text{Corollary 8.6.2}], A 5.1, A 5.3) \end{aligned}$$

2):

$$\begin{aligned} & \sigma_{\min}(\nabla_\theta^2 V_\alpha) \\ &= \sigma_{\min}\left(\frac{1}{\alpha^2} \nabla_\theta^2 [A^T A] + \frac{2}{\alpha} \nabla_\theta^2 [A^T B] + \nabla_\theta^2 [B^T B]\right) \\ &\geq \frac{1}{\alpha^2} \sigma_{\min}(\nabla_\theta^2 [A^T A]) - \sigma_{\max}\left(\frac{2}{\alpha} \nabla_\theta^2 [A^T B]\right) - \\ & \quad \sigma_{\max}(\nabla_\theta^2 [B^T B]) \quad ([14, \text{Equation 3.3.17}]) \end{aligned}$$

$$\begin{aligned}
&\geq \frac{1}{2\alpha^2} \sigma_{\min}(\nabla_{\theta}^2[A^T A](\theta_-)) - \sigma_{\max}(\frac{2}{\alpha} \nabla_{\theta}^2[A^T B] - \\
&\quad \sigma_{\max}(\nabla_{\theta}^2[B^T B])) \quad ([11, \text{Corollary 8.6.2}], A 5.1) \\
&\geq \frac{\sigma_X^2}{2\alpha^2} - \sigma_{\max}(\frac{2}{\alpha} \nabla_{\theta}^2[A^T B]) - \sigma_{\max}(\nabla_{\theta}^2[B^T B]) \quad (A 5.2) \\
&\geq \frac{\sigma_X^2}{2\alpha^2} - \frac{2}{\alpha} \sigma_{AB} - \sigma_{BB}. \quad ([11, \text{Corollary 8.6.2}], A 5.1, A 5.3)
\end{aligned}$$

3),4):

$$\begin{aligned}
\|\nabla_{\theta}^* G_{\alpha}\| &= \|\frac{1}{\alpha} \nabla_{\theta}^* A + \nabla_{\theta}^* B\| \\
&\leq \frac{1}{\alpha} \|\nabla_{\theta}^* A\| + \|\nabla_{\theta}^* B\| \quad (\text{triangle}) \\
&\leq \frac{1}{\alpha} M_A^* + M_B^*. \quad (A 5.1, A 5.3)
\end{aligned}$$

5),6),7):

$$\begin{aligned}
\|\nabla_{\theta}^* V_{\alpha}\| &= \|\frac{1}{\alpha^2} \nabla_{\theta}^* [A^T A] + \frac{2}{\alpha} \nabla_{\theta}^* [A^T B] + \nabla_{\theta}^* [B^T B]\| \\
&\leq \frac{1}{\alpha^2} \|\nabla_{\theta}^* [A^T A]\| + \frac{2}{\alpha} \|\nabla_{\theta}^* [A^T B]\| + \|\nabla_{\theta}^* [B^T B]\| \\
&\quad (\text{triangle}) \\
&\leq \frac{1}{\alpha^2} M_{AA}^* + \frac{2}{\alpha} M_{AB}^* + M_{BB}^*. \quad (A 5.1, A 5.3)
\end{aligned}$$

8):

$$\begin{aligned}
\|\nabla_{\theta} V_{\alpha}(\theta_-, w)\| &= \|\nabla_{\theta} G_{\alpha}(\theta_-)^T G_{\alpha}(\theta_-, w)\| \\
&= \|\frac{1}{\alpha} \nabla_{\theta} A(\theta_-) + \nabla_{\theta} B(\theta_-)\|^T B(\theta_-, w)\| \\
&\leq \frac{1}{\alpha} \|\nabla_{\theta} A(\theta_-)^T B(\theta_-, w)\| + \|\nabla_{\theta} B(\theta_-)^T B(\theta_-, w)\| \\
&\quad (\text{triangle}) \\
&\leq \frac{1}{\alpha} M_{AG} + M_{BG}. \quad (A 5.1, A 5.3)
\end{aligned}$$

9):

$$\|G_{\alpha}(\theta_-, w)\| \leq \frac{1}{\alpha} \|A(\theta_-)\| + \|B(\theta_-, w)\| = \|B(\theta_-, w)\| \leq M_G.$$

10): by A 5.1, A 5.3 and boundedness of feasible w . ■

Also in the region $\mathcal{B}(\theta_-, r)$, we have that Equation 9, Equation 7, and Algorithm 1 are well-defined because Lemma 9.1 implies that $\nabla_{\theta} G_{\alpha}$ is invertible:

Corollary 9.2: Assuming A 5.1, A 5.2, A 5.3, for r chosen as in Lemma 9.1, Algorithm 1 is well-defined as long as $\{\theta^k\} \subset \mathcal{B}(\theta_-, r)$.

We can easily show that in a small vicinity of θ_- , manifold projection always has a solution:

Theorem 9.3 (Continuous Convergence): Assuming A 5.1, A 5.2, A 5.3, for r chosen as in Lemma 9.1, there exists $\alpha_1 > 0$, such that for any $\alpha \leq \alpha_1$ and feasible w , the solution to $G_{\alpha}(\theta, w) = 0$ computed using the negative gradient flow $\dot{\theta} = -\nabla_{\theta} V_{\alpha}$ from initial guess θ_- is within $\mathcal{B}(\theta_-, r)$.

Proof: Solution Boundedness: Consider $V_{\alpha}(\theta, w) - V_{\alpha}(\theta_-, w)$, with $\theta \in \partial\mathcal{B}(\theta_-, r)$. We have strong convexity along line-segment connecting θ, θ^+ and by Lemma 9.1:

$$\begin{aligned}
&V_{\alpha}(\theta, w) - V_{\alpha}(\theta_-, w) \\
&\geq \nabla_{\theta} V_{\alpha}(\theta_-, w)^T (\theta - \theta_-) + (\frac{\sigma_X^2}{2\alpha^2} - \frac{2}{\alpha} \sigma_{AB} - \sigma_{BB}) \|\theta - \theta_-\|^2 \\
&\geq r^2 (\frac{\sigma_X^2}{2\alpha^2} - \frac{2}{\alpha} \sigma_{AB} - \sigma_{BB}) - r (\frac{1}{\alpha} M_{AG} + M_{BG}) = \mathcal{O}(\frac{1}{\alpha^2}).
\end{aligned}$$

If we choose small enough α_1 such that the last equation is larger than zero for all $\alpha \leq \alpha_1$, then V_{α} becomes a Lyapunov function of the gradient flow, restricting the solution to $\mathcal{B}(\theta_-, r)$ due to Nagumo's Theorem [3]. **Convergence:** We still need to show the gradient flow converges to a solution of $G_{\alpha}(\theta, w) = 0$, which is trivial due to the following inequality:

$$\begin{aligned}
\dot{V}_{\alpha} &= -\|\nabla_{\theta} V_{\alpha}\|^2 = -\|G_{\alpha}^T \nabla_{\theta} G_{\alpha} \nabla_{\theta} G_{\alpha}^T G_{\alpha}\| \\
&\leq -(\frac{\sigma_X}{2\alpha} - \sigma_B)^2 \|G_{\alpha}\|^2 = -(\frac{\sigma_X}{2\alpha} - \sigma_B)^2 V_{\alpha}.
\end{aligned}$$

We can again choose small enough α_1 such that the coefficient of V_{α} in the last inequality is smaller than zero. ■ Lemma 9.3 implies that, with sufficiently small α , PGM will always generate a sequence that is within $\mathcal{B}(\theta_-, r)$ if manifold projection is solved by exactly time-integrating the negative gradient flow.

B. Discrete First-Order Manifold Projection

In this section, we go beyond Lemma 9.3 and analyze the practical discrete manifold projection algorithm, i.e. Equation 9. Let's define the shorthand notation:

$$\theta^+ = \theta - \nabla_{\theta} G_{\alpha}^{-1} G_{\alpha}(\theta, w).$$

We first analyze the property of θ^+ , i.e. one iteration of manifold projection. We show that the relative change $\theta^+ - \theta$ is bounded:

Lemma 9.4: Assuming A 5.1, A 5.2, A 5.3, $V_{\alpha}(\theta, w) \leq M_V$ where M_V is some α -independent constant. For r chosen as in Lemma 9.1, there exists $\alpha_2 > 0$, such that for any $\alpha \leq \alpha_2$ and feasible w , $\|\theta^+ - \theta\| \leq r/2$ if $\theta^+, \theta \in \mathcal{B}(\theta_-, r)$.

Proof: If we choose $\alpha_2 \leq \alpha_1$:

$$\begin{aligned}
\|\theta^+ - \theta\| &= \|\nabla_{\theta} G_{\alpha}^{-1} G_{\alpha}\| \\
&\leq \|G_{\alpha}\| (\frac{\sigma_X}{2\alpha} - \sigma_B)^{-1} \leq \sqrt{M_V} (\frac{\sigma_X}{2\alpha} - \sigma_B)^{-1} \leq r/2.
\end{aligned}$$

The last inequality above holds by choosing small enough α_2 and the proof is complete. ■

We then show that it is possible to choose sufficiently small α such that the absolute norm of θ^+ is bounded:

Lemma 9.5: Assuming A 5.1, A 5.2, A 5.3, $V_{\alpha}(\theta, w) \leq M_V$ where M_V is some α -independent constant. For any $\beta \in (0, 1]$ and r chosen as in Lemma 9.1, there exists $\alpha_3(\beta) > 0$, such that for any $\alpha \leq \alpha_3(\beta)$ and feasible w , the following properties hold:

1) If $\theta \in \mathcal{B}(\theta_-, r\beta/2)$, then $\theta^+ \in \mathcal{B}(\theta_-, r\beta/2)$.

2) $V_{\alpha}(\theta^+, w) \leq 3V_{\alpha}(\theta, w)/4$.

Proof: Monotonic Reduction: As long as $\alpha \leq \alpha_3(\beta) \leq \alpha_2$, we have strong convexity over the line-segment connecting θ, θ^+ . This is because $\theta \in \mathcal{B}(\theta_-, r)$, $\theta^+ \in \mathcal{B}(\theta_-, r(1 + \beta)/2) \subset \mathcal{B}(\theta_-, r)$, and Lemma 9.1 implies strong convexity. By the Taylor's expansion theorem, we have:

$$\begin{aligned}
&V_{\alpha}(\theta^+, w) \\
&= V_{\alpha}(\theta, w) + \nabla_{\theta} V_{\alpha}^T (\theta^+ - \theta) + \\
&\quad \frac{1}{2} (\theta^+ - \theta)^T \nabla_{\theta}^2 V_{\alpha} (\theta^+ - \theta) + R_V \\
&= \frac{1}{2} (\theta^+ - \theta)^T \nabla_{\theta}^2 V_{\alpha} (\theta^+ - \theta) + R_V \\
&= \frac{1}{2} (\theta^+ - \theta)^T \sum_i \nabla_{\theta}^2 [G_{\alpha}]_i [G_{\alpha}]_i (\theta^+ - \theta) + R_V + \frac{1}{2} V_{\alpha}(\theta, w)
\end{aligned}$$

$$\begin{aligned}
&\leq \frac{1}{2} \left(\frac{1}{\alpha} M_A^2 + M_B^2 \right) \|\theta^+ - \theta\|^2 \|G_\alpha\| + \frac{1}{2} V_\alpha(\theta, w) + \\
&\quad \frac{1}{6} \left(\frac{1}{\alpha^2} M_{AA}^3 + \frac{1}{\alpha} M_{AB}^3 + M_{BB}^3 \right) \|\theta^+ - \theta\|^3 \\
&\leq \frac{1}{2} \left(\frac{1}{\alpha} M_A^2 + M_B^2 \right) \left(\frac{\sigma_X}{2\alpha} - \sigma_B \right)^{-2} V_\alpha(\theta, w)^{1.5} + \frac{1}{2} V_\alpha(\theta, w) + \\
&\quad \frac{1}{6} \left(\frac{1}{\alpha^2} M_{AA}^3 + \frac{1}{\alpha} M_{AB}^3 + M_{BB}^3 \right) \left(\frac{\sigma_X}{2\alpha} - \sigma_B \right)^{-3} V_\alpha(\theta, w)^{1.5} \\
&\leq \frac{1}{2} \left(\frac{1}{\alpha} M_A^2 + M_B^2 \right) \left(\frac{\sigma_X}{2\alpha} - \sigma_B \right)^{-2} \sqrt{M_V} V_\alpha(\theta, w) + \frac{1}{2} V_\alpha(\theta, w) + \\
&\quad \frac{1}{6} \left(\frac{1}{\alpha^2} M_{AA}^3 + \frac{1}{\alpha} M_{AB}^3 + M_{BB}^3 \right) \left(\frac{\sigma_X}{2\alpha} - \sigma_B \right)^{-3} \sqrt{M_V} V_\alpha(\theta, w) \\
&= \left(\frac{1}{2} + \mathcal{O}(\alpha) \right) V_\alpha(\theta, w),
\end{aligned}$$

where R_V is the residual term of the Taylor's expansion. We can choose $\alpha_3(\beta)$ small enough so that the coefficient of $V_\alpha(\theta, w)$ in the last inequality is smaller than $3/4$ for all $\alpha \leq \alpha_3(\beta)$. **Sequence Boundedness:** We prove $\theta^+ \in \mathcal{B}(\theta_-, r\beta/2)$ by contradiction. If we pick $\alpha_3(\beta)$ to ensure monotonic reduction, then $\theta^+ \in \mathcal{B}(\theta_-, r(\beta+1)/2)$ (Lemma 9.4). If $\theta^+ \notin \mathcal{B}(\theta_-, r\beta/2)$ then $\theta^+ \in \mathcal{B}(\theta_-, r(\beta+1)/2) - \mathcal{B}(\theta_-, r\beta/2)$. Since strong convexity holds along line segment connecting θ^+, θ_- , we have:

$$\begin{aligned}
&V_\alpha(\theta^+, w) - V_\alpha(\theta_-, w) \\
&\geq \nabla_\theta V_\alpha(\theta_-, w)^T (\theta^+ - \theta_-) + \left(\frac{\sigma_X^2}{2\alpha^2} - \frac{2}{\alpha} \sigma_{AB} - \sigma_{BB} \right) \|\theta^+ - \theta_-\|^2 \\
&\geq \frac{r^2 \beta^2}{4} \left(\frac{\sigma_X^2}{2\alpha^2} - \frac{2}{\alpha} \sigma_{AB} - \sigma_{BB} \right) - \frac{r(\beta+1)}{2} \left(\frac{1}{\alpha} M_{AG} + M_{BG} \right) \\
&\geq M_V.
\end{aligned}$$

Similarly, we can choose $\alpha_3(\beta)$ small enough so that the last inequality holds for all $\alpha \leq \alpha_3(\beta)$. This violates the fact that $V_\alpha(\theta^+, w) \leq 3V_\alpha(\theta_-, w)/4 \leq 3M_V/4$. ■

Now we have the desired convergence result as long as $V_\alpha(\theta, w)$ is upper bounded by some M_V , which is proved and the following theorem:

Theorem 9.6 (Discrete Convergence): Assuming

A 5.1, A 5.2, A 5.3, there exists some α -independent constant M_V , such that for r chosen as in Lemma 9.1, $\alpha_3(\beta)$ chosen as in Lemma 9.5, Algorithm 1 will generate a sequence $\{\theta^k, w^k\}$ with the following properties for all $\alpha \leq \alpha_3(\beta)$:

- 1) $\{V_\alpha(\theta^k, w^k)\}$ is upper bounded by M_V .
- 2) $\{\theta^k\}$ is within $\mathcal{B}(\theta_-, r\beta/2)$.
- 3) Each manifold projection is convergent at a rate of at least $3/4$.

Proof: We can proceed the proof by setting $M_V = M_G^2 + 2M_G M_{\Delta B} + M_{\Delta B}^2$. **Induction:** We prove by induction. The initial guess $V_\alpha(\theta^0, w^0) \leq M_V$ and $\theta^0 \in \mathcal{B}(\theta_-, r\beta/2)$. If $V_\alpha(\theta^{k-1}, w^{k-1}) \leq M_V$ and $\theta^{k-1} \in \mathcal{B}(\theta_-, r\beta/2)$, then Algorithm 1 will first update w^{k-1} to w^k and then update θ^{k-1} to θ^k via manifold projection. We use triangle inequality to bound the change of V_α due to the update of w as follows:

$$\begin{aligned}
&V_\alpha(\theta^{k-1}, w^k) - V_\alpha(\theta^{k-1}, w^{k-1}) \\
&= (G_\alpha(\theta^{k-1}, w^k) + G_\alpha(\theta^{k-1}, w^{k-1}))^T \\
&\quad (G_\alpha(\theta^{k-1}, w^k) - G_\alpha(\theta^{k-1}, w^{k-1})) \\
&\leq \left\| \left(\frac{2}{\alpha} A(\theta^{k-1}) + B(\theta^{k-1}, w^{k-1}) + B(\theta^{k-1}, w^k) \right) \right\| \\
&\quad \| (B(\theta^{k-1}, w^{k-1}) - B(\theta^{k-1}, w^k)) \| \text{ (triangle)} \\
&= \left\| \frac{2}{\alpha} A(\theta^{k-1}) + 2B(\theta^{k-1}, w^{k-1}) - B(\theta^{k-1}, w^{k-1}) + B(\theta^{k-1}, w^k) \right\|
\end{aligned}$$

$$\begin{aligned}
&\| (B(\theta^{k-1}, w^{k-1}) - B(\theta^{k-1}, w^k)) \| \\
&\leq 2 \| G_\alpha(\theta^{k-1}, w^{k-1}) \| \| B(\theta^{k-1}, w^{k-1}) - B(\theta^{k-1}, w^k) \| + \\
&\quad \| (B(\theta^{k-1}, w^{k-1}) - B(\theta^{k-1}, w^k)) \|^2 \text{ (triangle)} \\
&\leq 2M_G M_{\Delta B} + M_{\Delta B}^2,
\end{aligned}$$

so we have:

$$\begin{aligned}
V_\alpha(\theta^{k-1}, w^k) &\leq V_\alpha(\theta^{k-1}, w^{k-1}) + 2M_G M_{\Delta B} + M_{\Delta B}^2 \\
&\leq V_\alpha(\theta_-, w^{k-1}) + 2M_G M_{\Delta B} + M_{\Delta B}^2 \\
&\leq M_G^2 + 2M_G M_{\Delta B} + M_{\Delta B}^2 = M_V,
\end{aligned}$$

where in the last inequality we have used the fact that $\|G_\alpha(\theta^{k-1}, w^{k-1})\| \leq \|G_\alpha(\theta_-, w^{k-1})\|$. Next, we enter the phase of manifold projection. By Lemma 9.5, each step of manifold projection is reducing V_α at a rate of at least $3/4$ and staying inside $\mathcal{B}(\theta_-, r\beta/2)$. The proof is complete.

Solution Uniqueness: In the above proof we have used the fact that $\|G_\alpha(\theta^{k-1}, w^{k-1})\| \leq \|G_\alpha(\theta_-, w^{k-1})\|$. If we always start manifold projection from initial guess θ_- , then this is true due to Lemma 9.5. But if we start from any where in $\mathcal{B}(\theta_-, r\beta/2)$, this is also true because (1) Lemma 9.5 guarantees convergence; (2) Due to strong convexity Lemma 9.1, there is a unique solution to $V_\alpha = 0$ inside $\mathcal{B}(\theta_-, r\beta/2)$. ■ This result shows that all variables in Algorithm 1 are bounded and the manifold project substep is convergence.

C. Discrete Zeroth-Order Manifold Projection

The zeroth-order manifold projection can be proved to be convergent in an almost identical manner as that of Theorem 9.6 except for Lemma 9.5. We use the following shorthand notations:

$$\begin{aligned}
\theta^+ &= \theta - \nabla_\theta \bar{G}_\alpha^{-1} G_\alpha(\theta, w) \\
\Delta G &= \nabla_\theta G_\alpha - \nabla_\theta \bar{G}_\alpha \\
\Delta G_\alpha^{-1} &= \nabla_\theta G_\alpha^{-1} - \nabla_\theta \bar{G}_\alpha^{-1} \\
\nabla_\theta \bar{G}_\alpha^{-1} &= \nabla_\theta G_\alpha^{-1} - \Delta G_\alpha^{-1} \\
\nabla_\theta G_\alpha \Delta G_\alpha^{-1} &= \mathbf{I} - \nabla_\theta G_\alpha \nabla_\theta \bar{G}_\alpha^{-1} = -\Delta G \nabla_\theta \bar{G}_\alpha^{-1}.
\end{aligned}$$

The key to our proof is the fact that $\nabla_\theta G_\alpha$ and $\nabla_\theta \bar{G}_\alpha$ differs by an α -independent term. To proceed, we need to add the following results to Lemma 9.1:

Lemma 9.7: Assuming A 5.1, A 5.2, A 5.3, A 5.4, there exists an $r > 0$, such that for all feasible w , both Lemma 9.1 and the following properties hold within $\mathcal{B}(\theta_-, r)$:

- 1) $\sigma_{\min}(\nabla_w G \nabla_w G^T) \geq \sigma_w > 0$. (A 5.4)
- 2) $\|\nabla_w G \nabla_w G^T\| \leq M_w$.
- 3) $\sigma_{\min}(\nabla_\theta \bar{G}_\alpha) \geq \frac{\sigma_X}{2\alpha} - \bar{\sigma}_B$.
- 4) $\sigma_{\max}(\nabla_\theta G_\alpha \Delta G_\alpha^{-1}) \leq M_{\Delta G} \left(\frac{\sigma_X}{2\alpha} - \bar{\sigma}_B \right)^{-1}$.
- 5) $\sigma_{\max}(\Delta G_\alpha^{-1}) \leq \sigma_{\max}(\nabla_\theta G_\alpha^{-1}) \sigma_{\max}(\nabla_\theta G_\alpha \Delta G_\alpha^{-1}) \leq M_{\Delta G} \left(\frac{\sigma_X}{2\alpha} - \bar{\sigma}_B \right)^{-1} \left(\frac{\sigma_X}{2\alpha} - \sigma_B \right)^{-1}$.

We omit the proof which is similar to Lemma 9.1. Next, we prove the zeroth-order variant of Lemma 9.5 below:

Lemma 9.8: Assuming A 5.1, A 5.2, A 5.3, $V_\alpha(\theta, w) \leq M_V$ where M_V is some α -independent constant. For any $\beta \in (0, 1]$ and r chosen as in Lemma 9.1, there exists $\alpha_3(\beta) > 0$, such that for any $\alpha \leq \alpha_3(\beta)$ and feasible w , the following properties hold:

- 1) If $\theta \in \mathcal{B}(\theta_-, r\beta/2)$, then $\theta^+ \in \mathcal{B}(\theta_-, r\beta/2)$.

$$2) V_\alpha(\theta^+, w) \leq 3V_\alpha(\theta, w)/4.$$

Proof: Monotonic Reduction: As long as $\alpha \leq \alpha_3(\beta) \leq \alpha_2$, we have strong convexity over the line-segment connecting θ, θ^+ . By the Taylor's expansion theorem, we have:

$$\begin{aligned} & V_\alpha(\theta^+, w) \\ &= V_\alpha(\theta, w) + \nabla_\theta V_\alpha^T(\theta^+ - \theta) + \\ & \quad \frac{1}{2}(\theta^+ - \theta)^T \nabla_\theta^2 V_\alpha(\theta^+ - \theta) + R_V \\ &= V_\alpha(\theta, w) - \nabla_\theta V_\alpha^T \nabla_\theta \bar{G}_\alpha^{-1} G_\alpha + \\ & \quad \frac{1}{2}(\theta^+ - \theta)^T \nabla_\theta^2 V_\alpha(\theta^+ - \theta) + R_V \\ &= V_\alpha(\theta, w) - \nabla_\theta V_\alpha^T (\nabla_\theta G_\alpha^{-1} - \Delta G_\alpha^{-1}) G_\alpha + \\ & \quad \frac{1}{2}(\theta^+ - \theta)^T \nabla_\theta^2 V_\alpha(\theta^+ - \theta) + R_V \\ &= \nabla_\theta V_\alpha^T \Delta G_\alpha^{-1} G_\alpha + \frac{1}{2}(\theta^+ - \theta)^T \nabla_\theta^2 V_\alpha(\theta^+ - \theta) + R_V \\ &= \nabla_\theta V_\alpha^T \Delta G_\alpha^{-1} G_\alpha + \frac{1}{2} G_\alpha^T \nabla_\theta \bar{G}_\alpha^{-T} \nabla_\theta^2 V_\alpha \nabla_\theta \bar{G}_\alpha^{-1} G_\alpha + R_V \\ &= \nabla_\theta V_\alpha^T \Delta G_\alpha^{-1} G_\alpha + \frac{1}{2} G_\alpha^T (\nabla_\theta G_\alpha^{-1} - \Delta G_\alpha^{-1})^T \\ & \quad \nabla_\theta^2 V_\alpha (\nabla_\theta G_\alpha^{-1} - \Delta G_\alpha^{-1}) G_\alpha + R_V \\ &= \nabla_\theta V_\alpha^T \Delta G_\alpha^{-1} G_\alpha + \frac{1}{2} G_\alpha^T \nabla_\theta G_\alpha^{-T} \nabla_\theta^2 V_\alpha \nabla_\theta G_\alpha^{-1} G_\alpha + R_V + \\ & \quad \frac{1}{2} G_\alpha^T \Delta G_\alpha^{-T} \nabla_\theta^2 V_\alpha \Delta G_\alpha^{-1} G_\alpha - G_\alpha^T \Delta G_\alpha^{-T} \nabla_\theta^2 V_\alpha \nabla_\theta G_\alpha^{-1} G_\alpha \\ &= \nabla_\theta V_\alpha^T \Delta G_\alpha^{-1} G_\alpha + \frac{1}{2} V_\alpha(\theta, w) + R_V + \\ & \quad \frac{1}{2} G_\alpha^T \nabla_\theta G_\alpha^{-1} \sum_i \nabla_\theta^2 [G_\alpha]_i [G_\alpha]_i \nabla_\theta G_\alpha^{-1} G_\alpha + \\ & \quad \frac{1}{2} G_\alpha^T \Delta G_\alpha^{-T} \nabla_\theta^2 V_\alpha \Delta G_\alpha^{-1} G_\alpha - G_\alpha^T \Delta G_\alpha^{-T} \nabla_\theta^2 V_\alpha \nabla_\theta G_\alpha^{-1} G_\alpha. \end{aligned}$$

The above equation contains 5 terms other than $V_\alpha(\theta, w)/2$, we show that these terms are all $\mathcal{O}(\alpha)V_\alpha(\theta, w)$. The first term is:

$$\begin{aligned} & \|\nabla_\theta V_\alpha^T \Delta G_\alpha^{-1} G_\alpha\| \leq \|G_\alpha^T \nabla_\theta G_\alpha \Delta G_\alpha^{-1} G_\alpha\| \\ & \leq \|G_\alpha\|^2 M_{\Delta G} \left(\frac{\sigma_X}{2\alpha} - \bar{\sigma}_B\right)^{-1} = \mathcal{O}(\alpha)V_\alpha(\theta, w). \end{aligned}$$

The second term is:

$$\begin{aligned} \|R_V\| & \leq \frac{1}{6} \left(\frac{1}{\alpha^2} M_{AA}^3 + \frac{1}{\alpha} M_{AB}^3 + M_{BB}^3 \right) \\ & \quad \left(\frac{\sigma_X}{2\alpha} - \bar{\sigma}_B \right)^{-3} \sqrt{M_V} V_\alpha(\theta, w) = \mathcal{O}(\alpha)V_\alpha(\theta, w). \end{aligned}$$

The third term is:

$$\begin{aligned} & \left\| \frac{1}{2}(\theta^+ - \theta)^T \sum_i \nabla_\theta^2 [G_\alpha]_i [G_\alpha]_i (\theta^+ - \theta) \right\| \\ & \leq \frac{1}{2} \left(\frac{1}{\alpha} M_A^2 + M_B^2 \right) \|\theta^+ - \theta\|^2 \|G_\alpha\| \\ & = \frac{1}{2} \left(\frac{1}{\alpha} M_A^2 + M_B^2 \right) \left(\frac{\sigma_X}{2\alpha} - \bar{\sigma}_B \right)^{-2} \sqrt{M_V} V_\alpha(\theta, w) = \mathcal{O}(\alpha)V_\alpha(\theta, w). \end{aligned}$$

The fourth term is:

$$\begin{aligned} & \left\| \frac{1}{2} G_\alpha^T \Delta G_\alpha^{-T} \nabla_\theta^2 V_\alpha \Delta G_\alpha^{-1} G_\alpha \right\| \\ & \leq \left\| \frac{1}{2} G_\alpha^T \Delta G_\alpha^{-T} \nabla_\theta G_\alpha^T \nabla_\theta G_\alpha \Delta G_\alpha^{-1} G_\alpha \right\| + \\ & \quad \left\| \frac{1}{2} G_\alpha^T \Delta G_\alpha^{-T} \sum_i \nabla_\theta^2 [G_\alpha]_i [G_\alpha]_i \Delta G_\alpha^{-1} G_\alpha \right\| \\ & \leq \frac{1}{2} M_{\Delta G}^2 \left(\frac{\sigma_X}{2\alpha} - \bar{\sigma}_B \right)^{-2} V_\alpha(\theta, w) + \\ & \quad \frac{1}{2} \left(\frac{1}{\alpha} M_A^2 + M_B^2 \right) M_{\Delta G}^2 \left(\frac{\sigma_X}{2\alpha} - \bar{\sigma}_B \right)^{-2} \left(\frac{\sigma_X}{2\alpha} - \sigma_B \right)^{-2} \end{aligned}$$

$$\sqrt{M_V} V_\alpha(\theta, w) = \mathcal{O}(\alpha)V_\alpha(\theta, w).$$

The fifth term is:

$$\begin{aligned} & \|G_\alpha^T \Delta G_\alpha^{-T} \nabla_\theta^2 V_\alpha \nabla_\theta G_\alpha^{-1} G_\alpha\| \\ & \leq \|G_\alpha^T \Delta G_\alpha^{-T} \nabla_\theta G_\alpha^T G_\alpha\| + \\ & \quad \|G_\alpha^T \Delta G_\alpha^{-T} \sum_i \nabla_\theta^2 [G_\alpha]_i [G_\alpha]_i \nabla_\theta G_\alpha^{-1} G_\alpha\| \\ & \leq M_{\Delta G} \left(\frac{\sigma_X}{2\alpha} - \bar{\sigma}_B \right)^{-1} V_\alpha(\theta, w) + \\ & \quad \frac{1}{2} \left(\frac{1}{\alpha} M_A^2 + M_B^2 \right) M_{\Delta G} \left(\frac{\sigma_X}{2\alpha} - \bar{\sigma}_B \right)^{-1} \left(\frac{\sigma_X}{2\alpha} - \sigma_B \right)^{-2} \\ & \quad \sqrt{M_V} V_\alpha(\theta, w) = \mathcal{O}(\alpha)V_\alpha(\theta, w). \end{aligned}$$

The rest of the proof is the same as Lemma 9.5. Note that Theorem 9.6 holds in the zeroth-order case without A 5.4 because we have not used the condition $\sigma_{min}(\nabla_w G \nabla_w G^T) \geq \sigma_w > 0$. ■

D. First-Order PGM Convergence

The convergence of the first-order PGM is a trivial result of Theorem 9.6 and Taylor's expansion theorem.

Proof: [Theorem 5.5] If we set α_4 as in Theorem 9.6, then each θ^k satisfies $G(\theta^k, w^k) = 0$ and $K(\theta)$ can be expressed as a function of w , denoted as $K(w)$. Due to A 5.1 and A 5.3, $K(w)$ is differentiable and with gradient being:

$$\nabla_w K \triangleq -\nabla_w G^T \nabla_\theta G_\alpha^{-T} \nabla_\theta K.$$

From the optimality condition of Equation 8, we know that $\angle(\nabla_w K, \Delta w) \rightarrow \pi$ and $\Delta w \rightarrow 0$ as $\gamma \rightarrow 0$, so $\{K(\theta^k)\}$ is monotonically decreasing convergence is guaranteed. ■

E. Zeroth-Order PGM Convergence

The convergence proof of the zeroth-order PGM is a slight variant of the first-order Theorem 5.5. The key is to show that a descendent direction is always achieved with small enough α .

Proof: [Theorem 5.6] If we set $\alpha_5 \leq \alpha_4$ as in Theorem 9.6, then each θ^k satisfies $G(\theta^k, w^k) = 0$ and $K(\theta)$ can be expressed as a function of w , denoted as $K(w)$. Now we define the modified gradient:

$$\nabla_w \bar{K} \triangleq -\nabla_w G^T \nabla_\theta \bar{G}_\alpha^{-T} \nabla_\theta K.$$

From the optimality condition of Equation 10, we know that $\angle(\nabla_w \bar{K}, \Delta w) \rightarrow \pi$ and $\Delta w \rightarrow 0$ as $\gamma \rightarrow 0$. Next, we check whether $\nabla_w \bar{K}$ is also a descendent direction of $K(\theta^k)$:

$$\begin{aligned} & \|\nabla_w \bar{K}^T \nabla_w K\| \\ & = \|\nabla_\theta K^T \nabla_\theta \bar{G}_\alpha^{-1} \nabla_w G \nabla_w G^T \nabla_\theta G_\alpha^{-T} \nabla_\theta K\| \\ & = \|\nabla_\theta K^T \nabla_\theta G_\alpha^{-1} \nabla_w G \nabla_w G^T \nabla_\theta G_\alpha^{-T} \nabla_\theta K\| - \\ & \quad \|\nabla_\theta K^T \Delta G_\alpha^{-1} \nabla_w G \nabla_w G^T \nabla_\theta G_\alpha^{-T} \nabla_\theta K\| \\ & \geq \|\nabla_\theta K\|^2 \sigma_w \left(\frac{1}{\alpha} M_A^1 + M_B^1 \right)^{-2} - M_w \|\nabla_\theta K\|^2 \left(\frac{1}{\alpha} M_A^1 + M_B^1 \right)^{-1} \\ & \quad M_{\Delta G} \left(\frac{\sigma_X}{2\alpha} - \bar{\sigma}_B \right)^{-1} \left(\frac{\sigma_X}{2\alpha} - \sigma_B \right)^{-1} \text{ (Lemma 9.7, A 5.4)} \\ & = \mathcal{O}(\alpha^2) \|\nabla_\theta K\|^2 - \mathcal{O}(\alpha^3) \|\nabla_\theta K\|^2 \geq \mathcal{O}(\alpha^2) \frac{1}{2} \|\nabla_\theta K\|^2. \end{aligned}$$

The last inequality must hold by choosing small enough $\alpha_5 \leq \alpha_4$. The proof is complete. ■